Title

Inversion recovery ultrashort echo time magnetic resonance imaging: A method for simultaneous direct detection of myelin and high signal demonstration of iron deposition in the brain – A feasibility study

Authors

Sheth, Vipul R
Fan, Shujuan
He, Qun
et al.

Publication Date

2017-05-01

DOI

10.1016/j.mri.2016.12.025

Peer reviewed

HHS Public Access

Author manuscript

Magn Reson Imaging. Author manuscript; available in PMC 2017 July 10.

Published in final edited form as:

Magn Reson Imaging. 2017 May ; 38: 87–94. doi:10.1016/j.mri.2016.12.025.

Inversion Recovery Ultrashort Echo Time Magnetic Resonance Imaging: A Method for Simultaneous Direct Detection of Myelin and High Signal Demonstration of Iron Deposition in the Brain – A Feasibility Study

Vipul R. Sheth[1], **Shujuan Fan**[1], **Qun He**[1], **Yajun Ma**[1], **Jacopo Annesse**[2], **Robert Switzer**[3], **Jody Corey-Bloom**[4], **Graeme M Bydder**[1], and **Jiang Du**[1]

[1]Department of Radiology, University of California, San Diego, CA

[2]The Institute for Brain and Society, San Diego, CA

[3]NeuroScience Associates, Inc., Knoxville, TN

[4]Department of Neurosciences, University of California, San Diego

Abstract

Multiple sclerosis (MS)causes demyelinating lesions in the white matter and increased iron deposition in the subcortical gray matter. Myelin protons have an extremely short T_2* (less than 1 ms) and are not directly detected with conventional clinical magnetic resonance (MR) imaging sequences. Iron deposition also reduces T2*, leading to reduced signal on clinical sequences. In this study we tested the hypothesis that the inversion recovery ultrashort echo time (IR-UTE) pulse sequence can directly and simultaneously image myelin and iron deposition using a clinical 3T scanner. The technique was first validated on a synthetic myelinphantom (myelin powder in D2O) and a Feridex iron phantom. This was followed by studies of cadaveric MS specimens, healthy volunteers and MS patients. UTE imaging of the synthetic myelin phantom showed an excellent bi-component signal decay with two populations of protons, one with a T2* of 1.2 ms (residual water protons) and the other with a T2* of 290 μs (myelin protons). IR-UTE imaging shows sensitivity to a wide range of iron concentrations from 0.5 to ~30 mM. The IR-UTE signal from white matter of the brain of healthy volunteers shows a rapid signal decay with a short T2* of ~300 μs, consistent with the T2* values of myelin protons in the synthetic myelin phantom. IR-UTE imaging in MS brain specimens and patients showed multiple white matter lesions as well as areas of high signal in subcortical gray matter. This in specimens corresponded in position to Perl's diaminobenzide staining results, consistent with increased iron deposition. IR-UTE imaging simultaneously detects lesions with myelin loss in the white matter and iron deposition in the gray matter.

Keywords

myelin; iron; ultrashort echo time; magnetic resonance imaging; multiple sclerosis

Corresponding Address: Jiang Du, University of California, San Diego, Department of Radiology, 200 West Arbor Drive, San Diego, CA 92103-8756, Phone (619) 543-3512, Fax (619) 543-3736, jiangdu@ucsd.edu.

Introduction

Both myelin damage and iron deposition are the subjects of intensive investigation in multiple sclerosis (MS). MS is a disease that affects myelin, a lamellar membranous structure which contains alternating layers of protein and lipid. Iron is important in brain physiology and pathology. Iron accumulation occurs in the normal aging brain, particularly in the subcortical gray matter [1,2], and also in oligodendrocytes of the major white matter [3]. Researchers have observed abnormal iron deposition in the brain in MS, Parkinson's and Alzheimer's disease [4-7].

Both myelin and iron itself are not directly detected with conventional clinical magnetic resonance imaging (MRI) sequences. Myelin protons have extremely short T2*s (less than 1 ms), and the signal is not detected with conventional echo times (TEs) of 5 - 100 ms [8-12]. Myelin has been indirectly imaged using techniques such as myelin water fraction estimation by T2 relaxation fitting [11] and magnetization transfer imaging [12], in which signal is detected from water protons. Ultrashort echo time (UTE) MRI provides visualization of the very short T2*signal from protons in tissues such as cortical bone, menisci, ligaments, and tendons [8]. In addition, signals from myelin protons with T_2*s in the range of 50 μs to a few hundred microseconds are detectable with high performance NMR spectrometers [9,10].For example, using ultrashort echo time MRI techniques Horch et al recently showed signal components in the frog sciatic nerve, rat optic nerve, and bovine brain extract with T2 times of 50 μs to 1 ms which persisted after D2O exchange indicating likely origin from lipid components of myelin [9].

We have developed adiabatic inversion recovery UTE (IR-UTE) sequences with a minimum nominal TE of 8 μs that is 100-1000 times shorter than the TEs of most conventional clinical sequences, and these can potentially directly detect and image signals from myelin protons using clinical MR scanners [13-15]. The preparatory adiabatic inversion pulse is used to suppress signals from the long T2* components of white and gray matter. Furthermore, the IR-UTE sequences may also be sensitive to the short T2* signals associated with the presence of iron. Conventional iron sensitive MR imaging exploits changes in the transverse relaxation rates, R2 and R2*, and tissue susceptibility from deposited iron in the form of ferritin and hemosiderin [16,17], in which signal is detected from protons in water. However, these conventional sequences may show reduced signal when iron concentrations are too high and the T2*s of the associated water protons become too short. Typical concentration of iron in the brain ranges from 49 mg/kg in the thalamus to 205 mg/kg (equivalent to 1~4 mM) in the globus pallidus with estimated T2* of 14 – 40 ms [18].

Simultaneous imaging of myelin protons and iron deposition would be helpful in the diagnosis and treatment monitoring of MS and other neurological disease. In this study we tested the hypothesis that the inversion recovery ultrashort echo time (IR-UTE) pulse sequence could directly and simultaneously image myelin and iron deposition using a clinical 3T scanner. The technique was first validated on a synthetic myelin phantom (myelin powder in D2O) and a Feridex iron phantom, followed by studies of cadaveric MS

specimens and histological examination, as well as healthy human volunteers and patients with MS.

Methods

Pulse Sequences and Contrast Mechanisms

Figure 1 shows the pulse sequence and contrast mechanisms used in the IR-UTE sequence employed for simultaneous imaging of myelin and iron in vitro and in vivo in this study. The sequence employed a half-sinc radio frequency (RF) pulse (duration = 472μs, bandwidth = 2.7 kHz, flip angle = 60°), which together with variable rate selective excitation (VERSE), radial ramp sampling and fast transmit/receive switching reduced the nominal TE to 8 μs [8, 19]. In UTE imaging the long T2* components may have much higher signal intensity than the short T2* components. To create short T2* contrast, an adiabatic inversion pulse (duration = 8.64 ms, bandwidth ~ 1.5 kHz) preparation was used to invert and null signals from long T2* components in white matter (WM_L). Signals from myelin protons were nearly perfectly saturated because of their very short T2* (past simulation studies suggest that more than 95% of the signal being suppressed by the adiabatic IR pulse for short tissues, including myelin with T2*s in the order of 0.3 ms [14,15]) and thus significant transverse relaxation during the long adiabatic inversion process [19-21]. Subtraction of signals in the 2^{nd} echo image from those of the first echo image provided efficient suppression of residual longer T2* signals from long T2* gray matter (GM_L).The short T2* component of myelin were largely saturated by the adiabatic IR pulse, recovered during the inversion time (TI) and were detected by the UTE data acquisition. Iron deposition may lead to much reduced proton T2*s and T1s.The proton magnetization may be partially inverted or saturated by the adiabatic IR pulse [20], recover quickly during TI, and be detected by the UTE data acquisition. The IR-UTE sequence was implemented on a 3T Signa TwinSpeed Scanner (GE Healthcare, Milwaukee, WI). An eight-channel transmit/receive head coil was used.

Myelin and Iron Phantoms

Myelin Phantom Preparation—A 520 mg synthetic myelin lipid phantom approximating the nonprotein portion of biological myelin was prepared using a previously described procedure [13]. It consisted of 3:2 solid to liquid mass ratio of13.5% cholesterol, 13% galactocerebroside, 19.3% phosphatidylcholine, and 4.2% sphingomyelin (Sigma-Aldrich, St. Louis, MO) and deionized D2O which was mixed into a paste and placed in a glass NMR tube. The phantom was then subject to UTE imaging for T_2* measurement. A custom-made solenoid coil (5 mm in diameter) was used for signal excitation and reception. The following MR imaging parameters were used: field of view (FOV) = 4 cm, slice thickness = 3 mm, bandwidth (BW) = ±31.25 kHz, flip angle =60°, acquisition matrix = 128×128, number of projections = 403. For T2* measurements, a TR of 1000 ms and 14 TEs (8 μs, 0.1, 0.2, 0.4, 0.6, 0.8, 1.0, 1.2, 1.6, 2.0, 2.5, 3.2, 4.8, 6.4 ms) were used. A bi-component model (details below) was used to analyze the data.

Iron Phantom Preparation—The phantom consisted of seven tubes, each filled with 2 mL of Feridex I.V. solution (ferumoxides injectable solution, Berlex Laboratories, Wayne, NJ) in different concentrations (i.e., 2, 7.5, 15, 22.5, 30, 37.5 and 45 mM) which is broader

than typical iron concentration in the brain [18]. The tubes were placed in a cylindrical container (10 cm in diameter) filled with agarose gel (0.9% by weight).The longitudinal direction of the tubes was parallel to the B_0field.Similar parameters were used for the iron phantom studies, except for a larger FOV of 24 cm, a higher acquisition matrix of 256×256, a higher bandwidth of ±125 kHz, and a TI of 260 ms (chosen to null signals from long T2* agarose gel).Regular UTE without IR preparation and conventional clinical gradient-recalled echo (GRE) sequences were also applied to the iron phantom with similar imaging parameters for comparison.

MS Cadaver Brain Specimens

Five post-mortem brains from multiple sclerosis patient donors (2 male, 3 female, ages 28-71) were acquired from UCSD anatomical services within 24 hours of death. Brains were refrigerated (4 °C) until scanning when they were allowed to warm to room temperature for two hours prior to scanning. Typical imaging parameters were: TR = 1500ms, FOV = 24 cm, acquisition matrix =256×256, bandwidth = ±125 kHz, TE = 0.01/2.2 ms, slice thickness = 5 mm, flip angle = 60°, number of projections = 131, and sampling points per projection = 192.TIs varying between 400 and 450 ms were chosen to null WM_L based on the measured values of white matter T1.The scan time was 6.5 min. Clinical T_1- and T_2-weighted fast spin echo (FSE) sequences, T_2-weighted fluid attenuated inversion recovery (T_2-FLAIR) and magnetization prepared rapid acquisition gradient echo (MP-RAGE) sequences were also performed for comparison. The brains were refrigerated again after scanning was completed and returned to anatomical services for routine whole brain fixation within 48 hours.

Following MRI in the unfixed condition, the specimens were flotation-immersed in 10% buffered formalin and kept at room temperature for six months. The postmortem interval before fixation was less than 48hours. Samples were cryoprotected in graded solutions of sucrose (10-30%), then frozen in chilled isopentane and sectioned. Whole hemisphere slices were stored in 1M phosphate buffer before being mounted on large format glass slides for staining.

Perl's/Diaminobenzide (DAB) Stain—(NeuroScience Associates): Pre-cut sections were mounted on gelatin coated glass slides, air dried and passed through the following sequence: 95% ethanol/formaldehyde, 95% ethanol, 70% ethanol, rinsing in deionized water twice, Perl's Solution (2% hydrochloric acid + 2% potassium ferrocyanide), rinsing in deionized water three times, DAB H_2O_2 solution (DAB + phosphate buffered saline + 30% hydrogen peroxide), rinsing in deionized water three times, 70% ethanol, 95% ethanol, two changes of 100% ethanol, 1:1 100% ethanol/xylene, two changes of xylene, then cover slipped. Each slide was laser etched with the block number and the stain. Following serial ordering of the slides, they were numbered with ink in the upper right corner.

In Vivo Study

In total ten healthy volunteers (all male, ages 27-70) and ten MS patients (6 women and 4 men, ages 29-71) were recruited for this study, which was reviewed and approved by the Institutional Review Board (IRB) of the University of California, San Diego (UCSD). Written informed consent approved by the IRB was obtained prior to the participation of

each subject. The in vivo MRI protocol was similar to that used for the brain specimen study. In healthy volunteers, T_2* measurements were obtained by repeated IR-UTE acquisitions with five TEs (TE = 0.01, 0.2, 0.4, 0.6, 1.5 ms), requiring a total T_2* quantification time of 32 min. T2* measurements were not performed on the MS patients due to scan time limitation. Conventional clinical T_1- and T_2-weighted FSE sequences, T_2-FLAIR and MP-RAGE sequences applied to the brain specimens were also performed on healthy volunteers and MS patients for comparison.

Data Analysis

Quantitative evaluation of T_2* was performed on myelinphantoms and healthy volunteers using a Levenberg-Marquardt fitting algorithm written in Matlab R2011b (Math works Inc. Natick, MA, USA) and was executed offline on the DICOM images obtained using the protocols described above. The following single-component model was applied to the phantoms as well as in vivo studies:

$$S(TE)=S_0 \times e^{-TE/T2^*} \quad [1]$$

where S(TE) is the myelin signal with noise corrected using the Miller approach [22]:

$$<M(TE)^2>=S(TE)^2+2\sigma^2 \quad [2]$$

where<M(TE)^2> is the measured signal, and (&03C3) is the background noise calculated as the standard deviation of signal from a region of interest (ROI) drawn in air away from streaks.

For the myelin phantom study, the following bi-component analysis model was also employed to the normalized UTE signal S*(TE) to analyze the myelin proton T_2* ($T_{2,myelin}$*) and water proton T_2*($T_{2,water}$*) as well as their relative fractions F_{water} and F_{myelin} [23]:

$$S*(TE)=F_{\text{water}} \times e^{-TE/T^*_{2,\text{water}}}+F_{\text{myelin}} \times e^{-TE/T^*_{2,\text{myelin}}} \quad [3]$$

where F_{water} and F_{myelin} are the relative fractions of water protons and myelin protons, and are subject to the following constraint:

$$F_{\text{water}}+F_{\text{myelin}}=1 \quad [4]$$

The above bi-component model requires only three fitting parameters, which greatly reduces the sensitivity to signal to noise ratio (SNR) compared to the conventional five-parameter

fitting [24, 25]. After fitting was finished, goodness of fit statistics, including the R-squared value, mean squared error, root mean squared error, standard error and 95% confidence interval were calculated.

Results

The myelin phantom mimicked human physiologic myelin was prepared in D_2O to eliminate confounding signal from longer T2* protons in water or groups which exchange with water. The signal at various echo times was measured and fit to mono-exponential and bi-exponential models to estimate T2*. The mono-exponential model provided a T2* of 406 μs with relatively poor fitting ($R^2 = 0.9624$) of the experimental data,as compared with the bi-exponential model which showed excellent fitting ($R^2 = 0.9978$) with two populations of protons with T2*s of 290 μs and 1.2 ms (Figure 2).

The ability to detect the presence of iron with clinical GRE, UTE and IR-UTE sequences (Figure 3) was compared using Feridex suspension phantom. The clinical GRE sequence can detect iron with concentrations up to 2 mM. The UTE sequence can detect iron with concentrations up to 30 mM or higher. Improved iron contrast can be achieved with the IR-UTE sequence, where iron concentration up to 30 mM is visible. Off-resonance induced ringing artifacts are seen in samples with iron concentration above 30 mM.

In vivo IR-UTE imaging was also performed in otherwise healthy male volunteers. Figure 4 demonstrates selective imaging of short T2* white matter with high contrast in one subject. The calculated T2* of the white matter signal was 356 ± 47μs (Figure 4) which is similar in magnitude to the largest component detected with IR-UTE imaging of the myelin phantom where a T2* of ~290 μs was found (Figure 2).These results suggest that the myelin in white matter of the brain is being selectively imaged with the IR-UTE sequence.

Imaging of cadaver brains from patients with MS demonstrated high signal in areas of white matter (Figure 5A)on conventional T2-weighted images, consistent with MS plaques. These areas showeda loss of white matter signal on IR-UTE images (Figures 5 and 6). IR-UTE images in a 28-year-old with severe MS showed high signal in the globus pallidus and thalamus (Figure 5B)compared to that in other gray matter nuclei. There were also bilateral lesions extending from the globus pallidus to the thalamus. Figure 6 shows multiple slices from the cadaver specimen of a 65 year woman with MS. There are significant white matter abnormalities throughout the brain. In this specimen, high signal is seen in gray matter nuclei including the globus pallidus (Figure 6 F), substantianigra and red nucleus (Figure 6 E). In contrast, low signal intensity was seen in the cortical gray matter. Figure 7A shows coronal fixed frozen sections from the same patient illustrated in Figure 5. Corresponding IR-UTE imaging of the fixed section showed a hyper intense area (Figure 7B arrows) corresponding to the substantianigra and globus pallidus. Perl's-DAB staining of the same slice showed increased staining in the substantia nigra and globus pallidus consistent with increased iron deposition.

In vivo imaging of patients with MS using IR-UTE sequence demonstrated white matter lesions with high contrast (Figure 8), corresponding to or extending beyond lesions seen

with FLAIR and T1W sequences. In addition, in some patients with MS, there was also high signal demonstrated in the thalamus (Figure 8 F).This was also seen in some MS cadaver specimens (Figure 5B), consistent with iron deposition. These preliminary results demonstrate the feasibility of simultaneously directly imaging myelin and iron deposition in vivo.

Discussion

There has been debate about whether the ultrashort T2* signals are associated with myelin water. The signal shown in spectroscopy experiments is preserved after allowing exchange with D_2O [9], consistent with direct imaging of myelin rather than water. We show here that an ultrashort T2* signal is detected in myelin immersed in D_2O with IR-UTE sequence. This signal contains two components with estimated T2*s of ~300 μs and 1.2 ms (Figure 2). The T2* times reported here for myelin lipids are longer than those reported by Horch et al [9] or Wilhelm et al [10]. There are several potential reasons for this discrepancy. Our aqueous myelin phantoms may form lipid bilayers where the dipolar interactions scale the line shape, resulting in a superlorentzian shape [26]. Fitting with exponentials may result in overestimation of the T2*. In addition, our field strength of 3T is lower than that of the systems used by Horch (4.7T) and Willhelm (9.4T) [9,10]. The slice-selective excitation pulse used for brain specimens and in vivo imaging is relatively long at 472 μs, and we would expect signal decay during this pulse. However, the measured T2*s of the myelin lipid phantoms in D_2O and white matter components in specimens and in vivo imaged with IR-UTE are much shorter than the T2*s of myelin water which are approximately 10-20 ms [11]. This suggests that the signal source is the myelin lipid protons, though myelin associated water contamination cannot be completely excluded.

We also show that IR-UTE sequences generate a positive signal and are sensitive to higher concentrations of iron compared to conventional GRE sequences. The combined capabilities allow the IR-UTE pulse sequence to simultaneously detect white matter abnormalities and the effects of iron deposition in patients with MS. With IR-UTE sequences significant iron deposition appears high signal while white matter lesions appear as low signal. This may be an advantage of IR-UTE compared to other methods of measuring iron with MRI in which iron is typically hypo intense and so are areas of demyelination [27].

While MS is traditionally considered a disease of white matter, its involvement of gray matter and particularly the thalamus [28] is well known. This may be responsible for many of the clinical manifestations of MS including cognitive and motor dysfunction. Iron deposition may precede atrophy in thalamus [29]. In addition, it is widely recognized that iron in enriched within oligodendrocytes in both normal and diseased tissues [30]. Iron chelators have been shown to suppress symptoms in models of experimental allergic encephalitis [3]. Relatively decreased intensity on T2W images of putamen and thalamus may be related to increased iron accumulation (ferritin). This ferritin may be found in blood vessel walls, microglia, lysosome of glial cells, or oligodendrocytes [7]. Thus the form, location, and concentration of iron in the brain may play an important role in the clinical manifestations of multiple sclerosis. The IR-UTE sequence shows sensitivity to a wide range of iron concentrations compared with the conventional gradient echo based sequences.

While the IR-UTE sequence provides high contrast imaging of myelin and iron simultaneously, it can also easily separate myelin from iron by slightly adjusting the inversion time or TI. Myelin imaging is very sensitivity to TI. Selective myelin imaging is TI dependent. Inaccurate TI leads to water signal contamination. However, optimal TI can be determined by measuring T1 of the long T2 components, thus water contamination can be minimized. Iron signal is expected to be relatively insensitive to the variation in TI, as iron imaging relies on T1 shortening. The IR-UTE sequence can detect iron concentration up to 30 mM, which is much higher than the typical iron level in the brain. Iron has been implicated in many of the neurodegenerative diseases, including multiple sclerosis, Alzeimer's disease, Parkinson's disease, Huntington's disease, dementia with Lewy bodies, Hallervorden-Spatz disease (pantothenate kinase-associated neurodegeneration), etc. The associated abnormal gene-related iron absorption, transport and metabolism, age-related iron accumulation and abnormal iron-related protein deposits may lead to an increase in iron deposition in characteristic structures and locations, but typically less than 10 mM [31-35]. The IR-UTE sequence will be more effective than the conventional clinical sequences in the evaluation of iron overload associated with hemosiderosis, thalassemia, and sideroblastic anemia, where iron concentration more than 100 mM may be observed [36-38].

The phantom, specimens and in vivo volunteer and patient studies have confirmed our hypothesis that the IR-UTE sequence can simultaneously directly detect signal from myelin and iron deposition using a clinical 3T scanner. However, there are several limitations of this study. First, signal sources other than myelin protons (e.g., other macromolecules, myelin water due to imperfect nulling, etc.) may contribute to the IR-UTE signal, although the myelin phantom studies demonstrate that myelin protons are detectable with the IR-UTE sequence on a clinical 3T scanner. Second, additional work remains to be done to determine if we can also use IR-UTE to quantify iron in vivo. In addition, IR-UTE MRI sequence need to be compared to other methods of iron detection including SWI and QSM. Third, the IR-UTE sequence is two-dimensional, and is sensitive to eddy currents and gradient profile distortion [39]. Corrections of the residual slice-select gradients and time-varying main field $B_0(t)$ caused by eddy currents are required to reduce out-of-slice signal contamination [40].Three-dimensional UTE sequences such as adiabatic inversion recovery prepared Cones may find applications in volumetric mapping of myelin in vitro and in vivo [41]. By providing the simultaneous detection of myelin, MS lesions in white matter, and iron deposition in the gray matter, the IR-UTE sequence provides a new method of characterizing MS and potentially numerous other nervous system.

Acknowledgments

The authors acknowledge grant support from NIH (1R01 NS092650). VS was supported by the UCSD Clinician Scientist Program and NIBIB T32-EB005970.

References

1. Langkammer C, Krebs N, Goessler W, Scheurer E, Ebner F, Yen K, Fazekas F, Ropele S. Quantitative MR Imaging of Brain Iron: A Postmortem Validation Study. Radiology. 2010; 257:455–462. [PubMed: 20843991]

2. Hallgren B, Sourander P. The Effect of Age on the Non-Haemin Iron in the Human Brain. Journal of Neurochemistry. 1958; 3:41–51. [PubMed: 13611557]

3. LeVine SM, Macklin WB. Iron-enriched oligodendrocytes: a reexamination of their spatial distribution. J. Neurosci. Res. 1990; 26:508–512.

4. Stephenson E, Nathoo N, Mahjoub Y, Dunn JF, Yong VW. Iron in multiple sclerosis: roles in neurodegeneration and repair. Nat Rev Neurol. 2014; 10:459–468. [PubMed: 25002107]

5. Berg D, Youdim MBH. Role of iron in neurodegenerative disorders. Top MagnReson Imaging. 2006; 17:5–17.

6. LeVine SM. Iron deposits in multiple sclerosis and Alzheimer's disease brains. Brain Res. 1997; 760:298–303. [PubMed: 9237552]

7. Drayer B, Burger P, Hurwitz B, Dawson D, Cain J. Reduced signal intensity on MR images of thalamus and putamen in multiple sclerosis: increased iron content? AJR Am J Roentgenol. 1987; 149:357–363. [PubMed: 3496764]

8. Robson MD, Gatehouse PD, Bydder M, Bydder GM. Magnetic resonance: an introduction to ultrashort TE (UTE) imaging. J Comput Assist Tomogr. 2003; 27:825–846. [PubMed: 14600447]

9. Horch RA, Gore JC, Does MD. Origins of the ultrashort-T2 1H NMR signals in myelinated nerve: a direct measure of myelin content? MagnReson Med. 2011; 66:24–31.

10. Wilhelm MJ, Ong HH, Wehrli SL, Li C, Tsai PH, Hackney DB, Wehrli FW. Direct magnetic resonance detection of myelin and prospects for quantitative imaging of myelin density. Proc Natl Acad Sci USA. 2012; 109:9605–9610. [PubMed: 22628562]

11. MacKay A, Whittall K, Adler J, Li D, Paty D, Graeb D. In vivo visualization of myelin water in brain by magnetic resonance. MagnReson Med. 1994; 31:673–677.

12. Dousset V, Grossman RI, Ramer KN, Schnall MD, Young LH, Gonzalez-Scarano F, Lavi E, Cohen JA. Experimental allergic encephalomyelitis and multiple sclerosis: lesion characterization with magnetization transfer imaging. Radiology. 1992; 182:483–491. [PubMed: 1732968]

13. Waldman A, Rees JH, Brock CS, Robson MD, Gatehouse PD, Bydder GM. MRI of the brain with ultra-short echo-time pulse sequences. Neuroradiology. 2003; 45:887–892. [PubMed: 14508620]

14. Du J, Ma G, Li S, Carl M, Szeverenyi NM, VandenBerg S, Corey-Bloom J, Bydder GM. Ultrashort echo time (UTE) magnetic resonance imaging of the short T2 components in white matter of the brain using a clinical 3T scanner. Neuroimage. 2014; 87:32–41. [PubMed: 24188809]

15. Sheth V, Shao H, Chen J, Vandenberg S, Corey-Bloom J, Bydder GM, Du J. Magnetic resonance imaging of myelin using ultrashort echo time (UTE) pulse sequences: phantom, specimen, volunteer and multiple sclerosis patient studies. Neuroimage. 2016; 136:37–44. [PubMed: 27155128]

16. Haacke EM, Xu Y, Cheng YCN, Reichenbach JR. Susceptibility weighted imaging (SWI). MagnReson Med. 2004; 52:612–618.

17. Li L, Leigh JS. Quantifying arbitrary magnetic susceptibility distributions with MR. MagnReson Med. 2004; 51:1077–1082.

18. Bagnato F, Hametner S, Welch EB. Visualizingiron in multiple sclerosis. MagnReson Imaging. 2013; 31:376–384.

19. Du J, Carl M, Bydder M, Takahashi A, Chung CB, Bydder GM. Qualitative and quantitative ultrashort echo time (UTE) imaging of cortical bone. J MagnReson. 2010; 207:304–311.

20. Larson PE, Conolly SM, Pauly JM, Nishimura DG. Using adiabatic inversion pulses for long-T2 suppression in ultrashort echo time (UTE) imaging. MagnReson Med. 2007; 58:952–961.

21. Du J, Sheth V, Qun H, Carl M, Chen J, Corey-Bloom J, Bydder GM. Measurement of T1 of the ultrashort T2* components in white matter of the brain at 3T. PLoS ONE. 9(8):e103296.

22. Miller AJ, Joseph PM. The use of power images to perform quantitative analysis of low SNR MR images. MagnReson Imaging. 1993; 11:1051–1056.

23. Diaz E, Chung CB, Bae WC, Statum S, Znamirowski R, Bydder GM, Du J. Ultrashort echo time spectroscopic imaging (UTESI): an efficient method for quantifying bound and free water. NMR Biomed. 2012; 25:161–168. [PubMed: 21766381]

24. Reiter DA, Lin PC, Fishbein KW, Spencer RG. Multicomponent T2 relaxation analysis in cartilage. MagnReson Med. 2009; 61:803–809.

25. Bertero M, Boccacci P, Pike ER. On the recovery and resolution of exponential relaxation rates from experimental data: a singular-value analysis of the Laplace transform inversion in the presence of noise. Proc R Soc Lond A. 1982; 383:15–29.
26. Ulmius J, Wennerström H, Lindblom G, Arvidson G. Proton NMR bandshape studies of lamellar liquid crystals and gel phases containing lecithins and cholesterol. Biochim Biophys Acta. 1975; 389:197–202. [PubMed: 1138909]
27. Walsh AJ, Lebel RM, Eissa A, Blevins G, Catz I, Lu JQ, Resch L, Johnson ES, Emery DJ, Warren KG, Wilman AH. Multiple sclerosis: validation of MR imaging for quantification and detection of iron. Radiology. 2013; 267:531–542. [PubMed: 23297322]
28. Minagar A, Barnett MH, Benedict RHB, Pelletier D, Pirko I, Sahraian MA, Frohman E, Zivadinov R. The thalamus and multiple sclerosis: modern views on pathologic, imaging, and clinical aspects. Neurology. 2013; 80:210–219. [PubMed: 23296131]
29. Hagemeier J, Weinstock-Guttman B, Bergsland N, Heininen-Brown M, Carl E, Kennedy C, Magnano C, Hojnacki D, Dwyer MG, Zivadinov R. Iron deposition on SWI-filtered phase in the subcortical deep gray matter of patients with clinically isolated syndrome may precede structure-specific atrophy. AJNR Am J Neuroradiol. 2012; 33:1596–1601. [PubMed: 22460343]
30. Haacke EM, Makki M, Ge Y, Maheshwari M, Sehgal V, Hu J, Selvan M, Wu Z, Latif Z, Xuan Y, Khan O, Garbern J, Grossman RI. Characterizing iron deposition in multiple sclerosis lesions using susceptibility weighted imaging. J MagnReson Imaging. 2009; 29:537–544.
31. Quintana C, Bellefqih S, Laval JY, Guerquin-Kern JL, Wu TD, Avila J, FerrerI, Arranz R, Patino C. Study of the localization of iron, ferritin, and hemosiderin in Alzheimer's disease hippocampus by analytical microscopy at the subcellular level. J StructBiol. 2006; 153(1):42–54.
32. Stankiewicz J, Panter SS, Neema M, Arora A, Batt CE, Bakshi R. Iron in chronic brain disorders: imaging and neurotherapeutic implications. Neurotherapeutics. 2007; 4(3):371–386. [PubMed: 17599703]
33. Todorich B, Pasquini JM, Garcia CI, Paez PM, Connor JR. Oligodendrocytes and myelination: the role of iron. Glia. 2009; 57(5):467–478. [PubMed: 18837051]
34. Bartzokis G, Lu PH, Tishler TA, Fong SM, Oluwadara B, Finn JP, Huang D, Bordelon Y, Mintz J, Perlman S. Myelin breakdown and iron changes in Huntington's disease: pathogenesis and treatment implications. Neurochem Res. 2007; 32(10):1655–1664. [PubMed: 17484051]
35. Raven EP, Lu PH, Tishler TA, Heydan P, Bartzokis G. Increased iron levels and decreased tissue integrity in hippocampus of Alzheimer's disease detected in vivo with magnetic resonance imaging. J Alzheimers Dis. 2013; 37(1):127–136. [PubMed: 23792695]
36. Brittenham GM, Cohen AR, McLaren CE, Martin MB, Griffith PM, Nienhuis AW, Young NS, Allen CJ, Farrell DE, Harris JW. Hepatic iron stores and plasma ferritin concentration in patients with sickle cell anemia and thalassemia major. Am J Hematol. 1993; 42:81–85. [PubMed: 8416302]
37. Batts KP. Iron overload syndromes and the liver. Modern Pathology. 2007; 20:S31–S39. [PubMed: 17486050]
38. Taher AT, Musallam KM, Inati A. Iron overload: consequences, assessment, and monitoring. Hemoglobin. 2009; 33(S1):S46–57. [PubMed: 20001632]
39. Josan S, Pauly JM, Daniel BL, Pauly KB. Double half RF pulses for reduced sensitivity to eddy currents in UTE imaging. MagnReson Med. 2009; 61:1083–1089.
40. Lu A, Daniel BL, Pauly JM, Pauly KB. Improved slice selection for R2* mapping during cryoablation with eddy current compensation. J MagnReson Imaging. 2008; 28:190–198.
41. Carl M, Bydder GM, Du J. UTE imaging with simultaneous water and fat signal suppression using a time-efficient multispoke inversion recovery pulse sequence. Magn Reson Med. 2016; 76(2): 577–582. [PubMed: 26309221]

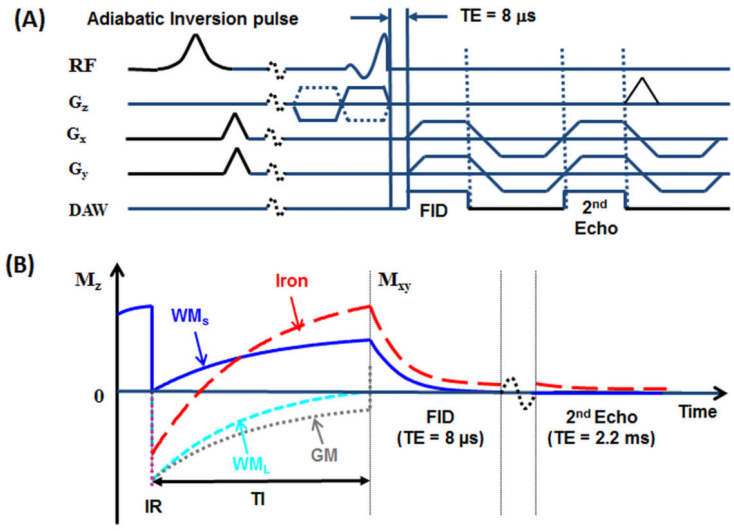

Figure 1.

(A) Diagram of IR-UTE MRI pulse sequence which employs a short half pulse excitation followed by dual echo radial ramp sampling with a minimal nominal TE of 8 μs. An adiabatic inversion pulse is used to invert and null signals from long T2 white matter (WM_L) and gray matter (GM). (B) Expected magnetization response of white and gray matter components and areas with iron deposition. TI is chosen so there is complete nulling of the long T2* white matter components (WM_L). The Short T2* white matter components (WM_S) are selectively imaged with UTE acquisition. Iron deposition is presumed to cause T1 shortening resulting in faster recovery and higher signal from adjacent protons (the amplitudes for WM_L, WM_S, GM and iron are non-scaled).

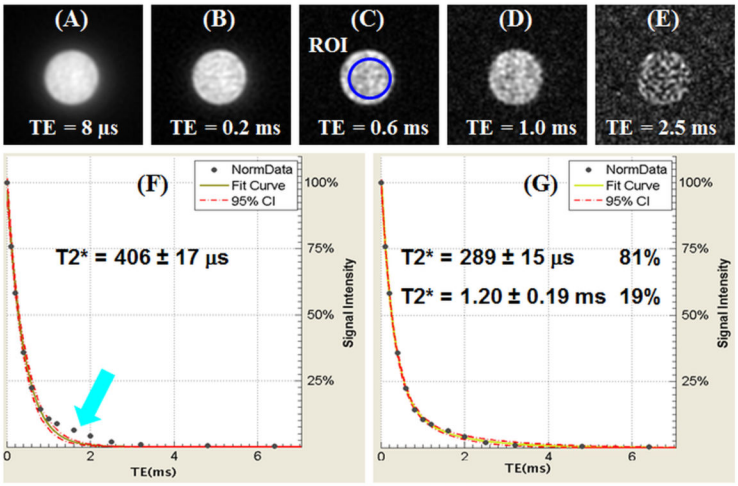

Figure 2.

Synthetic myelin phantom mimicking human physiologic myelin was prepared in D_2O. Imaging was performed with UTE MRI sequence without inversion pulse because preparation in D_2O was expected to eliminate signal from long T2 protons in water. The signal at various echo times was measured and fit to monoexponential and biexponential models to estimate T2* (A-E). The monoexponential model estimated a T2* of 406 us with poor fitting of the experimental data (F, blue arrow). The biexponential model showed good fitting with two populations of protons with T2* times of 1.2 ms and 290 us (G).

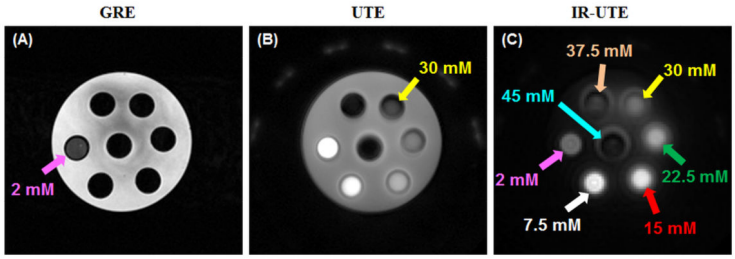

Figure 3.

Seven vials with different Feridex concentrations of 2, 7.5, 15, 22.5, 30, 37.5 and 45 mM were embedded in agarose gel and imaged with the GRE (A), UTE (B) and IR-UTE (C) sequences. The GREsequence can detect iron deposition up to 2 mM (A). Both the UTE (B) and IR-UTE (C) sequences can detect iron up to 30 mM. The IR-UTE sequence provides selective imaging of iron with efficient suppression of long T2 signal from agarose gel (C).

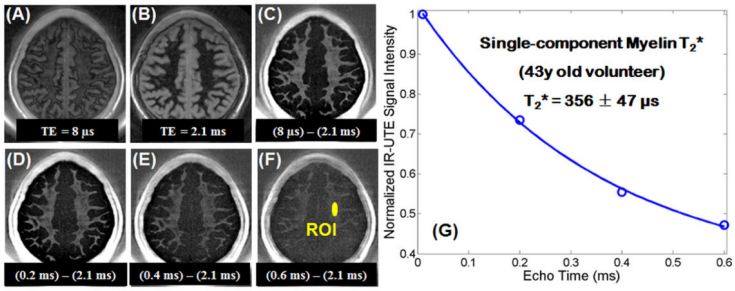

Figure 4.

Dual-echo IR-UTE imaging of a 43 years old healthy volunteer with TEs of 10 μs (A) and 2.2 ms (B), the corresponding echo subtraction image (C), and echo subtraction images from TEs of 0.2 ms (D), 0.4 ms (E) and 0.6 ms (F), as well as single-component T2* fitting (G) which shows a short T2* of 356 ± 47 us.

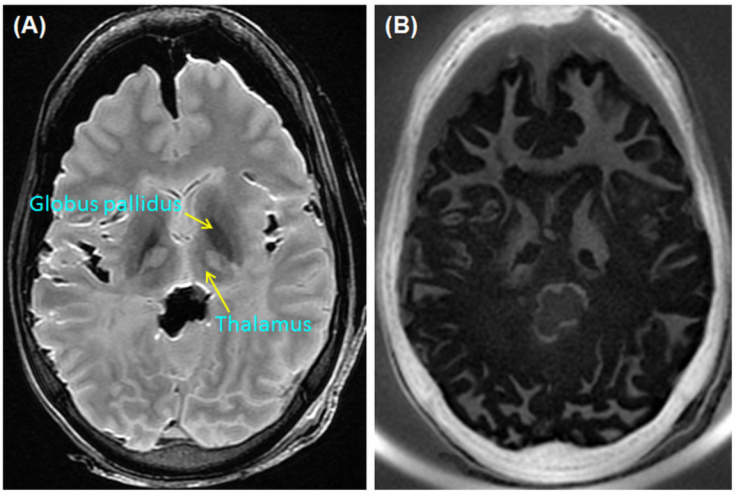

Figure 5.

Example image from cadaver brain of 28 years old woman with MS with high signal in areas of normal white matter on T2-FLAIR imaging consistent with multiple sclerosis lesions (A). Large areas of white matter abnormality on T2 weighted imaging corresponds to loss of white matter signal on the IR-UTE image (B). There is high signal in the thalamus and globuspalliduscompared to other gray matter nuclei (arrows). There are also bilateral lesions extending from the globuspallidus to the thalamus.

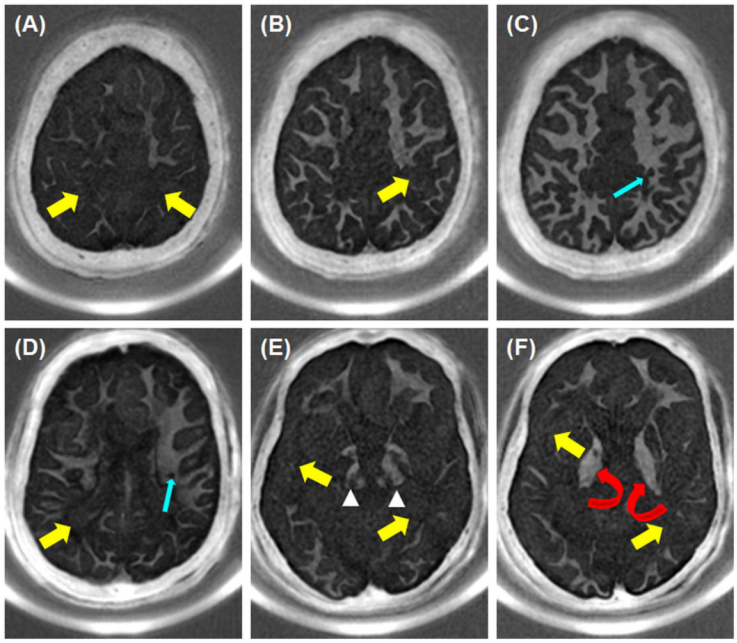

Figure 6.

Multiple slices from the cadaver specimen of a 65 years old woman with MS which show significant white matter abnormalities throughout the brain. Higher signal intensity is seen in some gray matter areas including the globuspallidus (curved arrows), substantianigra and red nucleus (arrow heads), areas known to have high iron deposition. Focal (thin arrows) and extensive (thick arrows) myelin loss were observed in white matter of the brain.

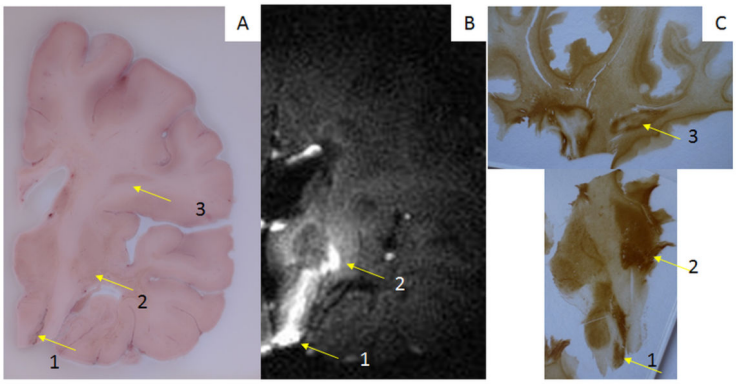

Figure 7.

(A) Unstained coronal fixed frozen section from 28 years old woman with MS. (B) Corresponding IR-UTE MRI image of fixed section (TR=100 ms, TI=50 ms). Image quality was limited due to changes in relaxation times post-fixation. (C) Perl's DAB stain of the same section at A & B show increased iron deposition in the substantianigra (1) and globuspallidus (2). Also note is a subcortical white matter multiple sclerosis lesion (3).

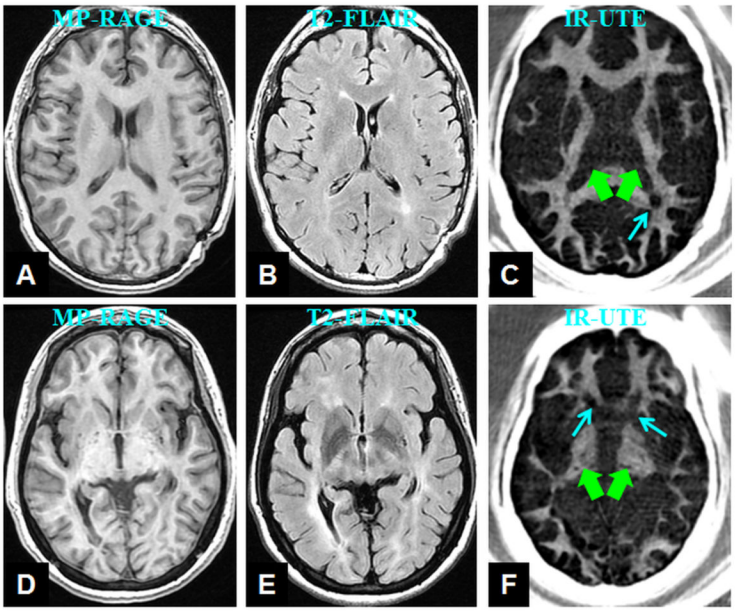

Figure 8.

Imaging of two patients with MS: a 37 years old man (A-C) and a 43 years old woman (D-F). MS lesions are clearly seen in both patients (thin arrows in C and F) with IR-UTE MRI. The thalamus shows high signal on the MP-RAGE image (D) and lower signal on the T2-FLAIR image (E), suggesting iron deposition. Higher contrast is seen on IR-UTE images which show high signal from the thalamus in the 43 years old patient compared with no signal in the thalamus in the 37 years old patient (thick arrows in F and C respectively).